Erosion Rate Estimates in Relation to Land-use Change: A Case Study in Samin Watershed, Central Java, Indonesia

Ekawati, N. L.,[1*] Danoedoro, P.[2] and Wibowo, S. B.[3]
Faculty of Geography, Universitas Gadjah Mada, Yogyakarta, Indonesia
E-mail: nur.lina.ekawati@mail.ugm.ac.id,[1*] pdanoedoro@ugm.ac.id,[2] sandy_budi_wibowo@ugm.ac.id[3]
**Corresponding Author*

DOI: https://doi.org/10.52939/ijg.v22i2.4789

Abstract
Soil erosion, as a critical land parameter, disrupts ecosystem balance. In alignment with Sustainable Development Goal 15 (life on land), mitigating land degradation is essential for maintaining environmental quality. Erosion estimations are empirically influenced by climate (R), soil properties (K), slope (LS), also vegetation cover and conservation practices (CP). Remote sensing is frequently used to estimate soil erosion, a phenomenon where soil material is transported by surface runoff, influenced by land-use changes driven by human activities. This study applies Random Forest classification to assess land-use as a CP-factor in estimating erosion rates in the Samin sub-watershed for 2017 and 2024, integrating spectral values from Landsat-8 and physical characteristics from Alos Palsar DSM. Samin sub-watershed, located upstream of Bengawan Solo watershed in Central Java, Indonesia, is part of volcanic landform of Lawu Volcano. R-factor was calculated for two distinct periods to account for its dynamic nature. The results of the R-factor range from 151.548 to 197.175 MJ.mm/ha.hour, the K-factor ranges from 0.23 to 0.42, the LS-factor ranges from 0.01 to 56.58, and the CP-factor values extracted from land use range from 0 to 1. The smallest CP value indicates low erosion potential, while higher values correspond to greater susceptibility to erosion. RUSLE model for 2017 ranges from 0 to 1984.9 tons/ha/year, and for 2024 ranges from 0 to 1174.61 tons/ha/year. A Pearson correlation analysis between erosion rate and CP-factor extracted from land use classification yields a coefficient of 0.95, indicating that 90% of the variation in the erosion rate is influenced by land use changes. Land areas without vegetation cover have high erosion potential, while dense vegetation exhibits lower erosion potential. Vegetation cover reduces the impact of rainwater by dissipating its energy, retaining and absorbing water, and decreasing surface runoff.

Keywords: Central Java, Land-Use, Random Forest, RUSLE, Soil Erosion,

1. Introduction

Critical land is defined as land that has been damaged due to changes in land-use, influenced by factors such as land cover, slope steepness, erosion hazard level, land productivity, and land management practices. According to the Decree of Indonesian Minister of Forestry (SK.328/Menhut-II/2009), 108 watersheds are experiencing land degradation, as indicated by critical land conditions including high erosion rates, critical hydrological levels, the need to protect vital infrastructure, disaster vulnerability, inappropriate agricultural practices, insufficient conservation efforts, and high population density [1]. Wischmeier and Smith (1978) by [1] states erosion as a natural phenomenon, occurs due to the breakdown and transportation of soil by surface water flow, defined as the movement of soil material influenced by water, caused by dispersion and transportation through surface runoff. This phenomenon negatively impacts land conditions, leading to the loss of fertile soil layers, reduced soil capacity to absorb and retain water, and a decline in the physical and chemical properties of the soil, all of which adversely affect plant growth [2]. Erosion can also result from human activities, such as agricultural practices that lead to the loss of the top-soil layer without adequate conservation measures, as well as development activities that damage the physical properties of the soil [3]. Morgan (2005) by [1] states that the erosion process occurs in three stages: detachment, transportation, and sedimentation, with the latter occurring when the available energy is insufficient to transport the soil material. Soil erosion

due to water movement is strongly influenced by climate change and the degradation of natural resources caused by inappropriate agricultural practices, deforestation, overgrazing, forest fires, and land development [4].

Limited land resources, when insufficiently managed to meet human needs, are often not accompanied by conservation efforts, which can lead to land degradation, including erosion [5][6] and [7]. Erosion resulting from human activities is often caused by the loss of topsoil due to agricultural practices that do not adhere to conservation principles, land-use changes, and development activities that damage ecosystems and reduce land productivity [7] and [8]. Erosion on agricultural land can degrade the hydraulic and physical properties of the soil, increasing the risk of drought, while low vegetation cover can further exacerbate erosion [9]. Critical land on steep slopes has a high erosion potential, while C-factor reflects the impact of vegetation cover and management practices on soil erosion in barren agricultural areas [10] and [11]. The erosion rate is typically expressed in tons/ha/year and can be modeled using the Revised Universal Soil Loss Equation (RUSLE) method to estimate average annual soil loss over a long period, considering surface runoff on a specific slope, land-use, and management system [12]. RUSLE, as an enhancement of the USLE method, uses the same parameters: rainfall characteristics, soil sensitivity to erosion, topography, land cover, and conservation practices, based on an empirical approach [1] and [12]. Several studies using the RUSLE model have shown that soil loss results from the combined effects of deforestation, overgrazing, inappropriate agricultural practices, expansion of agricultural land on steep slopes, and unsustainable natural resource utilization, leading to decreased soil productivity and increased food insecurity [13][14] and [15].

Remote sensing, as both science and art, involves the acquisition of information about the earth's surface and events through the analysis of data, using tools that do not require direct contact with the object of study [16]. Remote sensing plays a crucial role in determining the extent of erosion at different spatial scales. It helps identify and monitor erosion-prone areas at the regional level by utilizing spectral data, vegetation indices, and a combination of remote sensing and land morphology, provides valuable information on erosion factors, topography, soil properties, vegetation cover, and land-use [17]. Land-use, as a key parameter for assessing critical land, also serves as a crucial factor in determining erosion rates. Changes in land-use alter natural phenomena and ecological processes, influencing the dynamics of soil erosion and the resilience of the land, thereby affecting the method and intensity of soil erosion at various scales [18] and [19]. The Samin sub-watershed, located in the upstream area of the Bengawan Solo watershed, is a priority watershed covering 35,906 ha, primarily dominated by agricultural land use. Land-use mapping in this area presents several challenges, as multispectral digital classification is limited by spectral values, data normality, and the number of variables used. Additionally, land-use classification on diverse slopes necessitates the consideration of physical land characteristics. Classifying erosion rates based on land-use, the presence of vegetation cover is a key factor, random forest classification has shown high accuracy on complex landforms [20]. Furthermore, a combination of spectral values and terrain characteristics in random forest classification enables medium scale, multitemporal land use mapping, with the capability to identify up to 20 distinct land-use classes [21]. Random Forest, a non-parametric classification method based on a bootstrapping machine learning algorithm, is known for its robust predictive capacity, generating decision trees through random, iterative sampling procedures and predictions from individual decision trees, while also being notable for its ability to provide variable importance rankings, which are useful for identifying key variables in land cover classification [22] and [23].

Erosion rate estimation utilizes remote sensing technology, assuming that climate and land use factors are dynamic. Several raster-based erosion studies have been conducted by modeling vegetation indices to determine the C-factor, shown that incorporating soil spectral reflectance into vegetation indices results in a higher correlation compared to using vegetation indices alone, without considering soil reflectance [24] and [25]. Additionally, the combination of Digital Elevation Models (DEM) and vegetation indices provides a stronger correlation in determining the C-factor for erosion modeling [26]. Studies on erosion prediction have been conducted based on slope conditions and vegetation coverage, using Fractional Vegetation Cover (FVC) modeling for land cover and land use, with field validation results showing an accuracy of 67.92% [27]. In comparison, erosion prediction using an Artificial Neural Network (ANN) with parameters such as hidden layers, momentum, learning rate, and RMS, trained with a multi-layer perceptron and 9 layers of training data (a combination of erosion factors and four bands of SPOT-5 imagery), achieved the highest accuracy of 99.32%, which was significantly influenced by the number of iterations [28]. Land-use changes, driven by human needs, are mapped to determine the values of land cover factors and

conservation efforts. Land use classification for CP factor extraction, based on the integration of spectral values and physical characteristics using Random Forest, can provide better accuracy in classifying land use without the need to consider data normality. This study aims to estimate erosion rates in the Samin sub-watershed based on land-use classification as CP factors using Random Forest Classification for 2017 and 2024.

2. Materials and Methods

2.1 Study Area

The research location is the upstream area of the Bengawan Solo Watershed, covering an area of 35,906 ha, and spans parts of Karanganyar and Sukoharjo Regencies in Central Java, as shown in Figure 1. The Samin sub-watershed features a topography ranging from flat to mountainous relief, a tropical climate, and an average annual rainfall of 2,500 mm/year. The soil types in the area include lithosol, andosol, mediterranean, and regosol. The upstream section is located on Lawu Volcano, with land-uses including forests, agriculture, plantations, and settlements. The combination of land-use changes and diverse management practices has contributed to its classification as a critical watershed.

2.2 Data

This research was conducted using Landsat 8 imagery with a spatial resolution of 30 m, utilizing spectral values from the blue, green, red, Near-IR, and Short Wave-IR bands, along with the Alos Palsar DSM for elevation and slope steepness. Landsat imagery was used to monitor various land features, with visible bands for general monitoring, and Near-IR and SW-IR bands providing spectral values for vegetation, land conditions, built-up areas, soil, and minerals [29][30] and [31]. Landsat 8 has a 12-bit radiometric resolution and has an image scene area of 185 x 185 km [32] and [33]. The Alos Palsar (Advanced Land Observing Satellite Synthetic Aperture Radar) DSM, provided by the Alaska Satellite, uses a microwave sensor with an L-band and has an effective spatial resolution of 12.5 m. This DSM is useful for morphometric studies and soil erosion research [34] and [35]. The Landsat 8 images on August 15, 2017, and August 18, 2024, and the Alos Palsar DSM were recorded on August 27, 2009. The Alos Palsar DSM was used to ensure a consistent assessment of erosion rate estimates based on land-use changes, as no major geomorphological events affected the topography of the Samin sub-watershed during the study period.

2.3 Methods

Erosion rate estimation was conducted using an empirical approach, with influencing factors including climate, soil, slope, and land-use. Remote sensing is utilized to extract information related to these supporting factors. The estimation was made by integrating Landsat imagery and Alos Palsar DSM to determine the relationship between erosion rates and land-use changes (Figure 2). Erosion rates in the Samin sub-watershed were estimated using the RUSLE method. Monthly rainfall was used to calculate R-factor, while soil properties determining K-factor were analyzed in the laboratory.

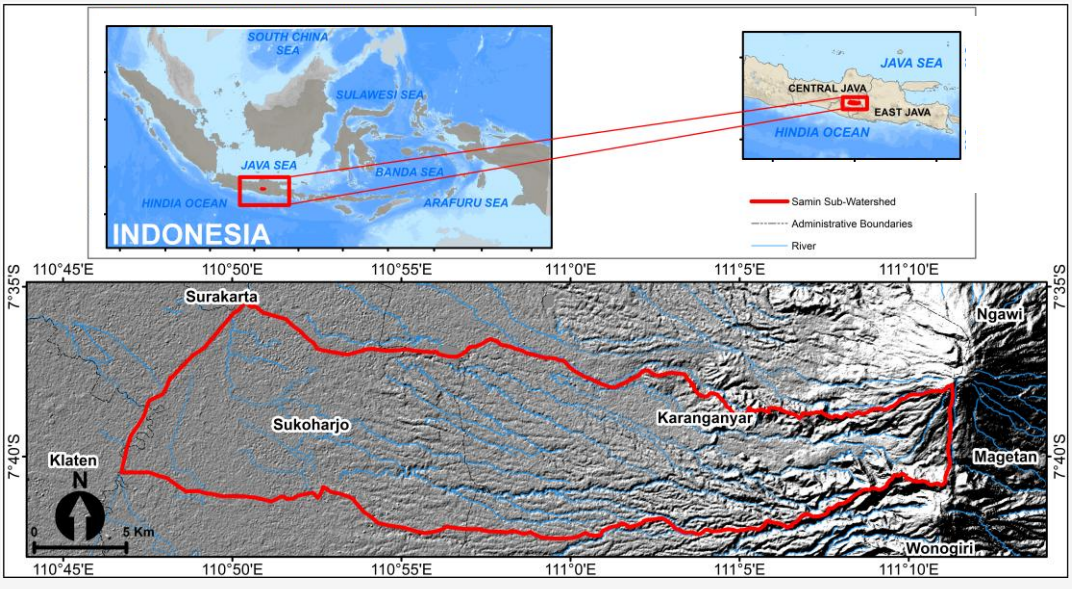

Figure 1: Study area

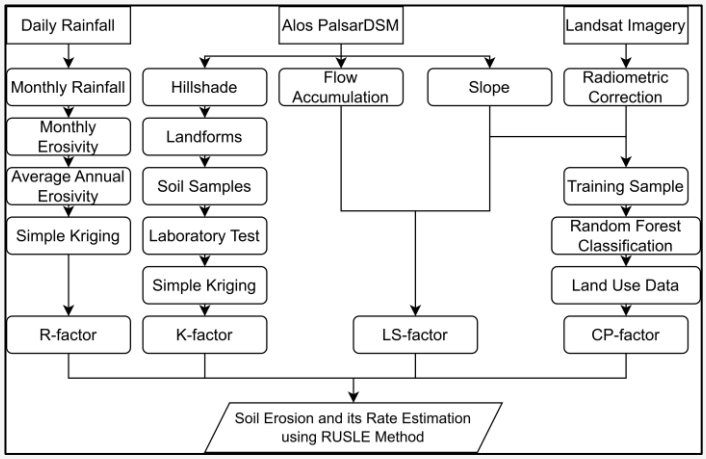

Figure 2: Research flowchart

The LS-factor was derived from the Alos Palsar DSM through flow accumulation and slope steepness, and land-use classification from Landsat imagery using Random Forest provided the CP-factor. Erosion rates were estimated for 2017 and 2024, assuming changes only in the CP-factor, while the R-factor was applied dynamically for both periods. The empirical approach is presented in Equation 1:

$$A = R \cdot K \cdot L \cdot S \cdot C \cdot P$$

Equation 1

Where A is soil erosion (ton/ha/year), R is rain erosivity (MJ.mm/ha/hour), K is soil erodibility, L is slope length, S is slope steepness, C is vegetation cover, P is conservation practices.

2.3.1 Rain erosivity (R-Factor)

Rain erosivity is a parameter used to quantify the amount of rainfall energy, specifically at a 30-minute rainfall intensity, that influences the soil erosion rates. However, due to the limited availability of rain gauges in Indonesia, several modifications have been made to the calculation of rain erosivity. In this context, daily rainfall data was utilized to estimate monthly rainfall, then used to calculate the monthly and annual rain erosivity [3]. The approach as described by [1], is based on the use of monthly rainfall data, represented by Equation 2:

$$R = 2.21P^{1.36}$$

Equation 2

Where R is rain erosivity (MJ.mm/ha/hour), P is monthly rainfall (cm).

2.3.2. Soil Erodibility (K-Factor)

Soil erodibility refers to the soil's susceptibility to erosion, which is determined by its physical and chemical properties. It is calculated based on the soil's structure, texture, permeability, and organic matter content. Erodibility is also influenced by topographic conditions and human activities [1]. Soil structure and permeability are classified according to their physical characteristics and laboratory test results, as described by [1] in Table 1 and Table 2. Meanwhile, the United States Department of Agriculture (1973) by [2] classifies soil erodibility into six categories, as shown in Table 3.

Table 1: Soil structure

Soil Structure (diameter size)	Code
Very fine granular (<1mm)	1
Fine granular (1-2 mm)	2
Medium to coarse granular (2-10 mm)	3
Blocks, plates, and massifs	4

Table 2: Soil Permeability

Permeability	Rate (cm/hour)	Code
Very slow	<0.5	6
Slow	0.5 – 2.0	5
Slow to moderate	2.0 – 6.3	4
Moderate	6.3 – 12.7	3
Moderate to fast	12.7 – 25.4	2
Fast	>25.4	1

Table 3: Soil erodibility

Erodibility	K value	Code
Very low	0.00 – 0.10	1
Low	0.11 – 0.21	2
Moderate	0.22 – 0.32	3
A bit high	0.33 – 0.44	4
High	0.45 – 0.55	5
Very high	0.56 – 0.64	6

The calculation of soil erodibility is given by Equation 3:

$$K = \frac{[23.71 \times 10^{-4} (12 - C_a) M^{1.14} + 4.20(S_t - 2) + 3.23(P_r - 3)]}{100}$$

Equation 3

Where K is soil erodibility, C_a is organic matters, M from soil fraction, S_t is structure, P_r is permeability.

2.3.3 Slope length and slope steepness (LS-Factor)

Slope length is measured from the starting point of surface flow to the endpoint of soil deposition, which occurs due to the reduction in slope and the surface flow entering the river. The slope steepness is used to assess the amount of erosion on a plot of land with a specific slope and its effect on the surface flow volume [1]. LS factor modeling considers both the flow accumulation and the slope steepness, as well as the pixel size applied. Moore and Burch (1985) by [36] formulated the *LS* factor for spatial modeling, as expressed in Equation 4:

$$LS = \left(\frac{A_s c}{22.13} \right) \left(\frac{\sin \theta}{0.0896} \right)^n$$

Equation 4

Where A_s is flow accumulation, c is cell size, θ is slope steepness (degree), m is 0.6, and n is 1.3.

2.3.4 Vegetation cover and conservation practices CP-Factor)

Land cover factors determine the magnitude of erosion based on vegetation cover, while conservation measures reflect the reduction in erosion through decreased runoff, achieved by altering the direction and pattern of surface flow [1]. Remote sensing was used to model the CP factor without direct field contact, overcoming limitations related to the lack of detailed field data. Landsat imagery provides spectral reflectance values of land cover, while the Alos Palsar DSM offers elevation data. The CP factor was assessed based on nine land-use classes, following the modified Wischmeier and Arnoldus classification by [1], with the average combined CP factor values listed in Table 4. Land-use classification was performed by integrating Landsat imagery with the Alos Palsar DSM, using Random Forest classification. The variables used in the classification include blue, green, red, Near-IR, and Short Wave-IR bands, as well as the Alos Palsar DSM and slope steepness. The training samples were extracted from polygon boundaries of pixels representing each land-use class, with classification performed using default settings, where *ntree* = 500 and *mtry* = 2.

Table 4: Land-use and CP-values

Vegetation Cover and Conservation Practices	CP-values
Water body	0.00
Built-up area	0.00
Bare land	1.00
Forest	0.18
Agriculture	0.10
Shrub and grass	0.03
Plantation	0.21
Mixed cropland	0.44
Terraced cropland	0.25

2.3.5 Erosion rate estimation using RUSLE method

The estimation of erosion rates was achieved by integrating the R, K, LS, and CP factors using an empirical approach, expressed in tons/ha/year. The relationship between erosion rates and land-use changes can have both positive and negative impacts. It is well-established that the presence of vegetation cover plays a critical role in preventing soil transport by surface runoff. Erosion rate estimations were made by integrating Landsat imagery and the Alos Palsar DSM. Erosion rates were classified into five hazard classes according to the Regulation of the Indonesian Director General of Watershed and Protected Forest Control No. P.3/PDASLH/SET/KUM.1/7/2018 [1], as shown in Table 5.

Table 5: Erosion hazard level

Erosion Rate	Soil Loss Erosion (ton/ha/year)	Class
I	< 15	Very light
II	15 – 60	Light
III	60 – 180	Moderate
IV	180 – 480	Heavy
V	> 480	Very heavy

3. Results

3.1 Rain Erosivity

Rainfall erosivity modeling calculates monthly rainfall using the Lenvain equation, with erosivity values derived from the annual averages for two periods: 2008-2016 for the 2017 period and 2015-2023 for the 2024 period. The calculated rainfall erosivity for 2017 ranges from 139.61 to 259 MJ.mm/ha/hour and for 2024 ranges from 127.29 to 289.73 MJ.mm/ha/hour. The highest rainfall erosivity is observed at P.10 in Tawangmangu rainfall station, while the lowest erosivity occurs at P.5 in Purwantoro and P.8 in Klaten rainfall stations. Variation in average annual rainfall and erosivity is presented in Figure 3. It was shown that a strong relationship exists between rainfall and rain erosivity in the Samin sub-watershed, where higher rainfall corresponds to higher erosivity.

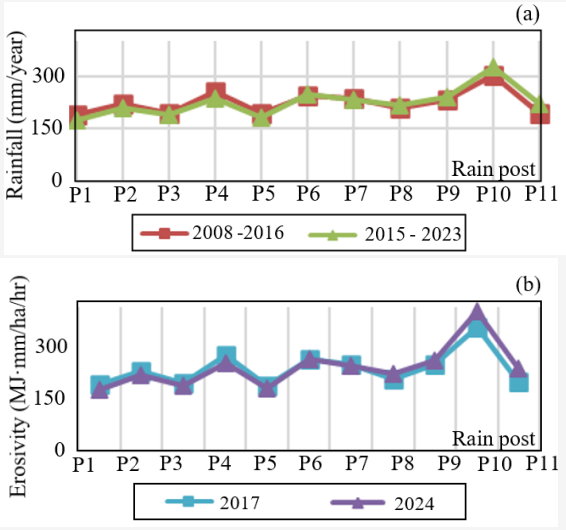

Figure 3: (a) annual rainfall, and (b) rain erosivity

Spatial modeling is performed using the simple kriging method, which accounts for spatial correlation and semi variograms. Spatial correlation is used to determine the distribution of data by establishing lag spacing. If the lag spacing is too small or too large, the data may not be representative, so a lag spacing of 4500 is applied. Determining the nugget, sill, and range parameters is necessary for fitting a semivariogram in geostatistical analysis, as more accurate parameter estimates lead to a better representation of the spatial dependence of each point. For 2017, the nugget was 1750, the sill 3250, and the range 60000. For 2024 model, the nugget was 4750, the sill 6300, and the range 60000.

The results of the rainfall erosivity modeling for Samin sub-watershed are as follows: in 2017 ranged from 172.921 to 197.174 MJ.mm/ha/hour and in 2024 ranged from 182.152 to 194.003 MJ.mm/ha/hour. Autocorrelation analysis and rainfall erosivity model results are shown in Figures 4 and 5.

3.2 Soil Erodibility

The erodibility factor represents the soil's susceptibility to erosion, which is influenced by its physical and chemical properties, as determined through laboratory tests. Erodibility samples were selected based on landforms identified through visual interpretation, as shown in Figure 6. A total of 20 soil samples were collected, considering topographic variations. Undisturbed samples are used for permeability tests, while disturbed samples are used for testing structure, texture, and soil organic matter content. Soil texture reflects the dominant fractions, which are classified on the soil texture triangle, with clay being the dominant fraction in the study area. The M texture was calculated based on the percentage of soil fractions, with the lowest value of 395.7 observed from the lower slopes of old volcanoes (101), and the highest value of 7486.5 recorded from the young volcanic slopes (96). The soil structure ranged from very fine granular to blocky in dry soils, indicating the degree of particle aggregation. Soil permeability tests assess the soil's ability to transmit water, with values ranging from 0.22 to 29.75 cm/hour, where higher values correspond to faster water permeability.

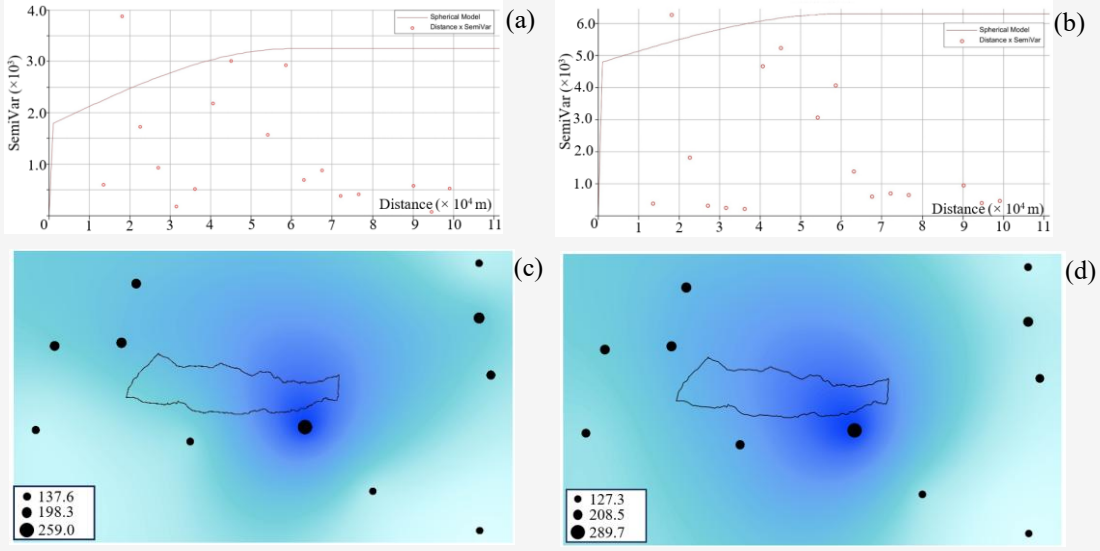

Figure 4: Erosivity interpolation (a) semivariogram of 2008 – 2016 (b) semivariogram of 2015 – 2023 (c) rainfall erosivity surface of 2008- 2016 (d) rainfall erosivity surface of 2015- 2023

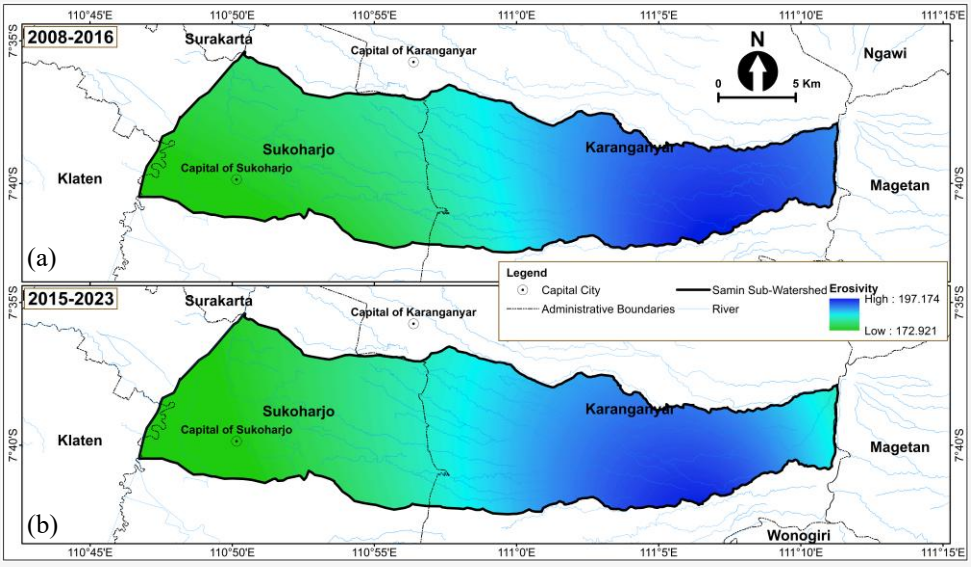

Figure 5: R-Factor (a) 2008 – 2018, and (b) 2015 - 2023

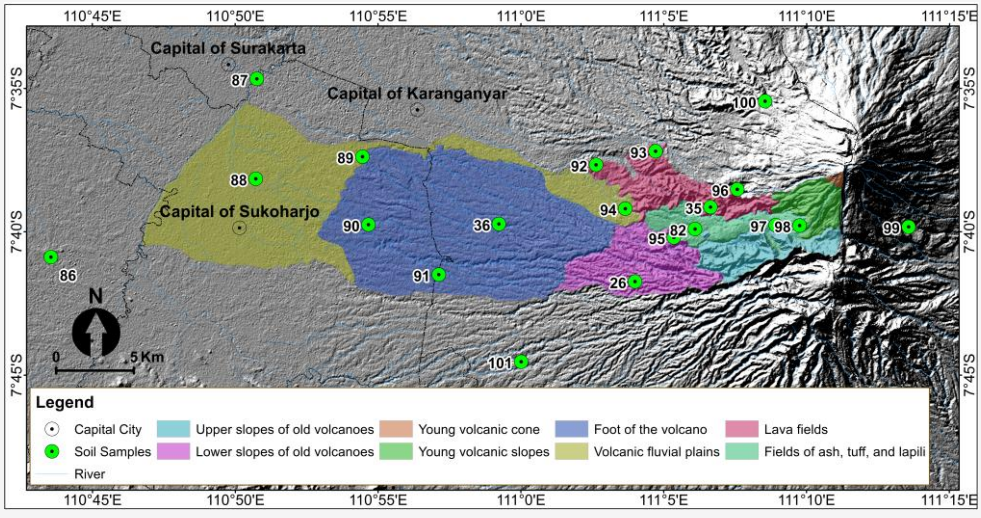

Figure 6: Soil samples based on Samin Sub-watershed landform units

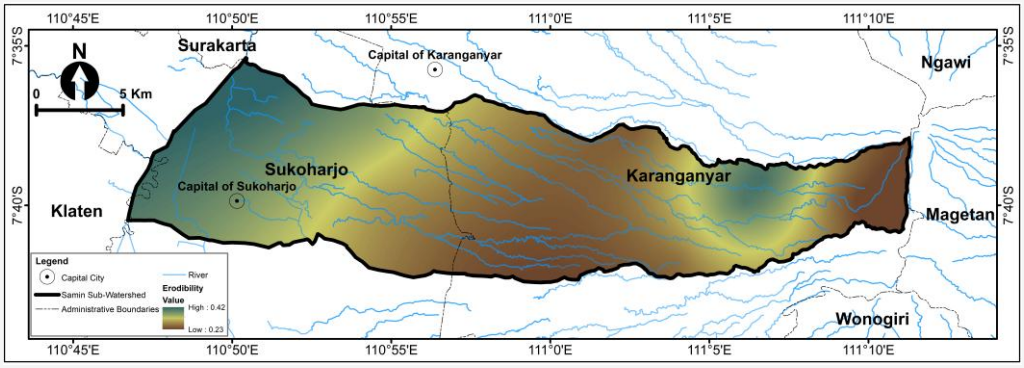

Figure 7: K-Factor

Table 8: Soil laboratory results

Sample	Soil Fraction (%)			Class	M	Structure	Permeability	OM	K Factor
	Sand	Silt	Clay		Texture				
26	6.21	25.67	68.12	Clay	1,016.46	3	3.36	2.56	0.14
35	26.23	43.33	30.43	Clay Loam	4,839.75	3	1.68	1.21	0.57
36	5.76	22.46	71.78	Clay	796.32	4	0.22	2.71	0.23
82	39.64	43.93	16.43	Loam	6,984.04	3	7.39	3.71	0.58
86	22.61	47.68	29.71	Clay Loam	4,941.20	3	13.04	2.43	0.43
87	14.18	60.44	25.38	Silt Loam	5,568.23	3	3.26	3.06	0.53
88	21.16	36.82	42.02	Clay	3,362.21	3	0.90	2.51	0.38
89	32.99	34.27	32.74	Clay Loam	4,524.31	3	2.24	3.05	0.43
90	10.06	32.24	57.69	Clay	1,789.83	4	6.55	3.16	0.21
91	19.88	29.84	50.27	Clay	2,472.93	3	9.30	2.80	0.23
92	11.13	24.87	64.00	Clay	1,296.20	3	25.37	1.90	0.11
93	7.02	30.77	62.21	Clay	1,428.02	3	0.78	1.28	0.22
94	44.12	23.09	32.79	Clay Loam	4,517.27	2	29.76	2.41	0.32
95	29.92	29.51	40.57	Clay	3,531.93	3	0.63	1.82	0.41
96	43.89	42.64	13.48	Loam	7,486.50	2	2.13	4.18	0.59
97	32.49	38.24	29.27	Clay Loam	5,002.06	1	24.90	6.89	0.15
98	31.92	15.19	52.89	Clay	2,219.31	3	29.41	7.01	0.07
99	25.15	26.29	48.56	Clay	2,645.98	1	1.74	6.47	0.14
100	22.87	40.31	36.81	Clay Loam	3,992.46	2	3.66	6.93	0.21
101	6.06	13.83	80.11	Clay	395.70	4	1.84	1.89	0.17

High organic matter content from ash fields, tuff, and lapilli (98) indicates a greater capacity to resist erosion, while low organic matter content from lava fields (93) suggests a higher susceptibility to erosion. The K factor was determined from soil laboratory test, with values ranging from 0.07 to 0.59, as shown in Table 8.

K factor modeling using simple kriging interpolation accounts for spatial autocorrelation analysis by adjusting the nugget, sill, and range parameters. The range of K factor values for the Samin sub-watershed spans from 0.23 to 0.42, with the highest values observed in the volcanic fluvial plains and the western side of the volcanic slopes. The lowest values are observed on the slopes of both old and young volcanoes, as well as the western side of the volcanic foothills. Higher soil erodibility corresponds to greater susceptibility to erosion, as soils with high erodibility are more easily transported by surface runoff. Conversely, soils with low erodibility are more resistant to erosion. The K-factor is shown in Figure 7.

3.3 Slope Length and Slope Steepness

The assessment of the LS factor was based on topographic conditions, where the magnitude of the slope indicates the vulnerability to erosion when rainfall impacts the soil. LS factor modeling accounts for both the flow accumulation and the slope steepness, illustrating the direction and volume of flow across the land. The steepest slope flow direction was applied to represent the movement of water from steeper to gentler slopes. The flow accumulation in the Samin sub-watershed ranges from 1 to 213344 cells, with the highest accumulation occurring in the volcanic fluvial plain downstream. Slope steepness is presented in degrees, with classifications ranging from flat to very steep. The steepest slopes are found in the Lawu Volcano area, while the volcanic fluvial plain exhibits flatter terrain. The upper reaches of the watershed feature very steep slopes, which gradually flatten as one move downstream. The LS parameter is shown in Figure 8. The LS factor modeling considers a pixel size of 30 m, with values ranging from 0.01 to 56.58. The highest values are observed on volcanic slopes, while the lowest values are found on volcanic fluvial plains. The upper reaches of the watershed exhibit larger values, which decrease as the topography becomes flatter. Steeper slopes correspond to higher LS factor values, while areas with higher flow accumulation tend to have smaller LS factor values. The LS-factor model is shown in Figure 9.

3.4 Vegetation Cover and Conservation Practices

The erosion rates are influenced by land use and vegetation coverage, with vegetated land being more resilient to erosion. Standing vegetated land, when combined with appropriate land conservation practices, can reduce erosion potential through a root system that stabilizes the soil and mitigates surface runoff. The conversion of land use to CP values was adjusted according to the classification of CP value forecasts in Java. Agriculture is used to define mixed and home gardens, which are associated with built-up areas. Mixed cropland refers to agricultural systems with diverse crop types, while terraced cropland represents agriculture involving terracing

conservation and irrigated rice cultivation.

Land-use data was classified using Random Forest model, which involves building multiple decision trees and applying bootstrapping machine learning to rank variable importance. Random Forest classification was conducted by integrating eight variables: spectral bands from Landsat 8 and terrain characteristics represented by the ALOS PALSAR DSM and its derivatives. Table 9 shows that the SWIR band had the most significant influence on land use modeling in 2017, while the variable with the least influence was slope steepness. In contrast to 2017, in 2024, the blue band had the greatest influence compared to other classification variables, while slope steepness remained the least influential. The classification results for 2017 showed a model accuracy of 81.07% compared to the training samples, while the 2024 classification had a model accuracy of 76.83%. The modeling results were then validated in the field, with an overall field accuracy of 87.74% for 2017 and 92.01% for 2024.

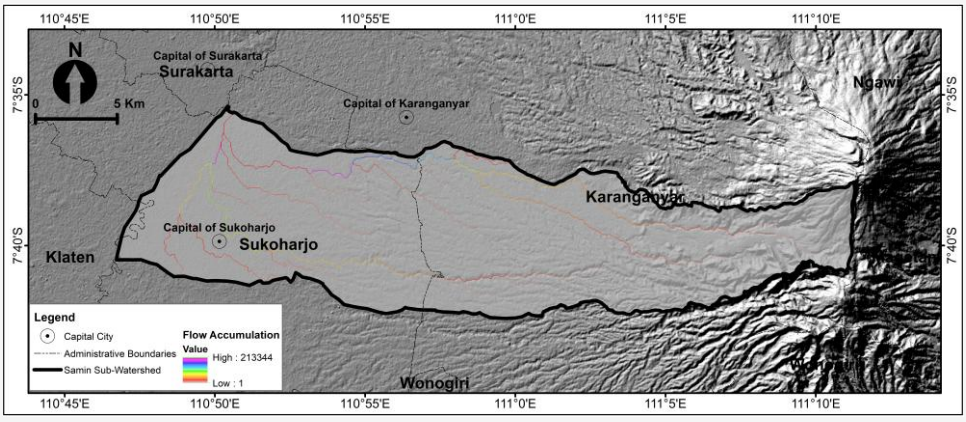

(a)

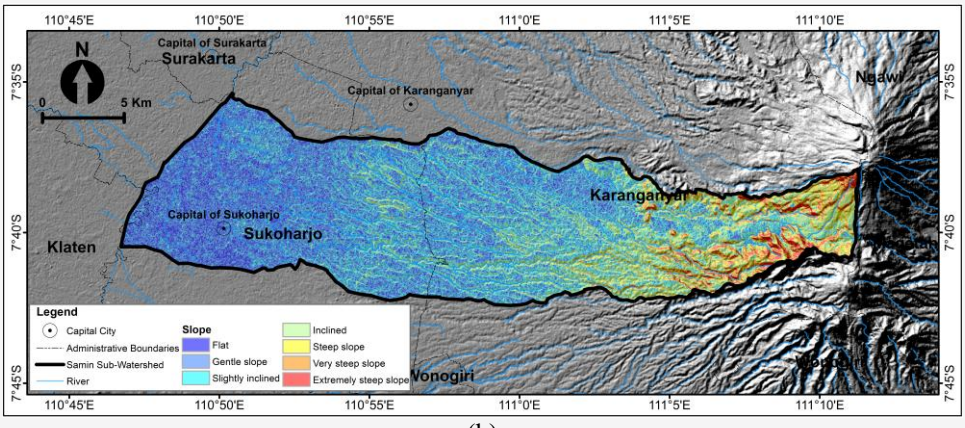

(b)

Figure 8: LS Parameter (a) flow accumulation, and (b) slope steepness

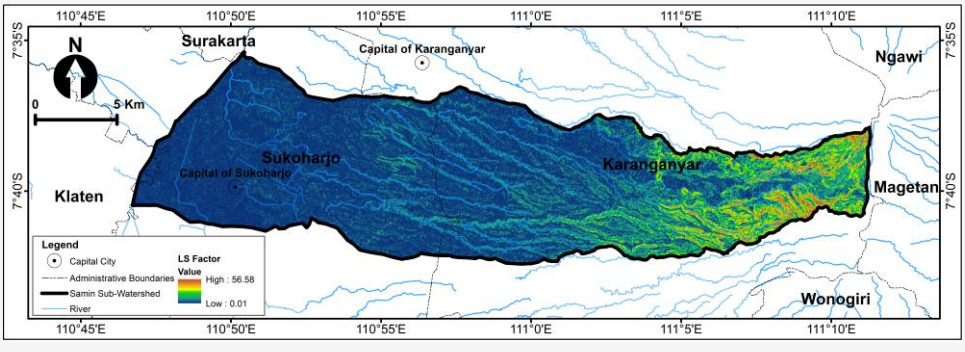

Figure 9: LS-Factor

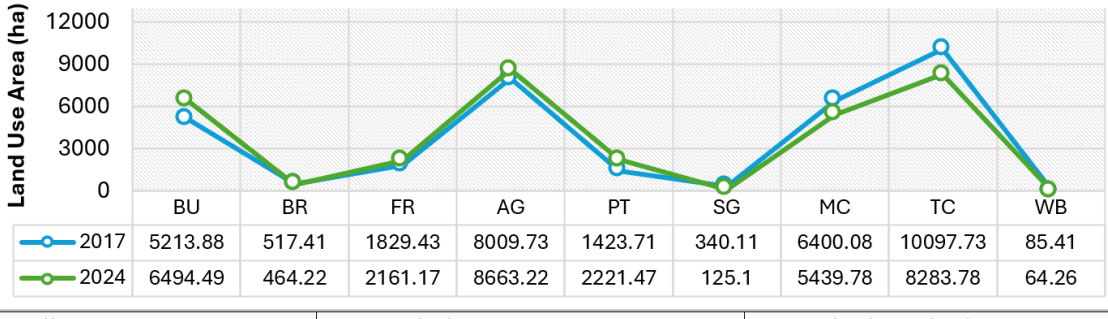

BU: Built-up	AG: Agriculture	MC: Mixed Cropland
BR: Bare land	PT: Plantations	TC: Terraced Cropland
FR: Forests	SG: Shrubs and Grasses	WB: Water Body

Figure 10: Land-use changes

The results indicate that built-up areas, forests, agricultural land, and plantations increased between 2017 and 2024, while other land-use types decreased. These changes in land-use classification may be attributed to alterations in land appearance and low spectral value differentiation. The decline in cropland, coupled with the increase in built-up areas, reflects the growing demand for development. Water bodies, including rivers and other aquatic features, as well as terraced cropland, experienced significant decreases due to the similarity in spectral values between inundated terraced cropland and water bodies, making these two land-use types difficult to distinguish. The increase in forests is accompanied by a decrease in agricultural land, with both land use types categorized based on the type of woody vegetation. These land uses differ in their associations, as agriculture (mixed and yard areas) is directly associated with built-up areas, while forests are linked to terraced cropland on volcanic slopes. Figure 10 illustrates that vegetated land dominates 70%of the study area, with cropland being a significant component.

Table 9: Variable importance random forest classification

Bands	2017	2024
Blue	926.52	3,258.67
Green	603.24	2,351.22
Red	824.76	2,437.38
NIR	952.31	1,496.43
SWIR 1	1,102.44	1,518.93
SWIR 2	1,443.62	1,761.09
DEM Alos Palsar	1,308.36	2,941.09
Slope	262.57	515.52

Land-use classification is shown in Figure 11, indicates that shrubs and grasses dominate the upper stream. Mixed cropland, agriculture, and plantations are predominant on the western slopes of Lawu Volcano, while mixed cropland, built-up areas, and terraced cropland dominate the lower slopes of Lawu Volcano and the downstream volcanic fluvial plain of the sub-watershed. Modeling with a spatial resolution of 30 m results in less detailed classification outcomes, such as in the case of water bodies, where only the Bengawan Solo River Channels is identifiable. Bare land became clearly visible in 2017, while forests began to be more distinguishable in 2024. Terraced agricultural land decreased towards the center of Karanganyar Regency by 2024. Mixed cropland, associated with agriculture, appears to have declined as agricultural land expanded.

The CP factor for each land use was assessed by converting it to a value from 0 to 1, where 0 represents land with low erosion potential, influenced by dense vegetation cover and conservation efforts, while 1 represents land devoid of vegetation cover, making it highly susceptible to erosion (see Table 4). Water bodies and built-up areas do not experience erosion, as water bodies function as sedimentation zones, and built-up areas cover the entire land surface, thereby reducing the extent of land affected by soil erosion. Forests, agriculture, and shrub grasses exhibit relatively low CP values, while plantations and cropland areas exhibit higher CP values due to the low density of standing vegetation. The highest CP value is found in bare land, as it lacks vegetation to mitigate erosion caused by rainfall and surface runoff. The modeling shown in Figure 12 indicates that, in 2024, a wider yellow area is observed, suggesting an increase in land with no erosion potential.

Blue areas represent regions with high erosion potential, located at the foot and fluvial plains of volcanoes, while volcanic slopes are predominantly by green, indicating moderate erosion potential. Overall, slope areas are characterized by moderate erosion potential, while the foot and fluvial plains of the volcano exhibit higher erosion potential.

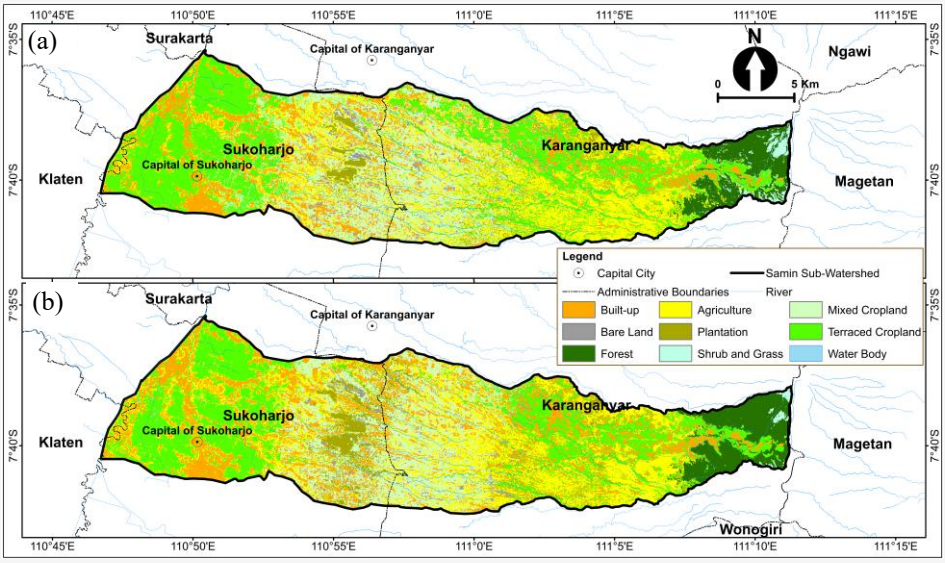

Figure 11: Land-use (a) 2017, and (b) 2024

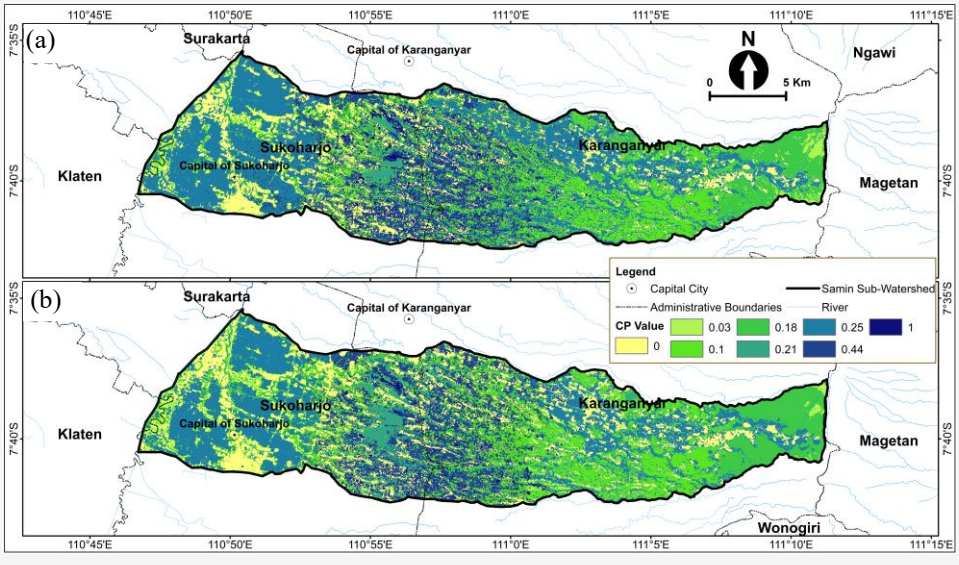

Figure 12: CP-Factor (a) 2017, and (b) 2024

3.5 Soil Erosion Estimation using RUSLE Method

Erosion estimation, using the RUSLE method, is expressed in tons/ha/year through the integration of the R, K, LS, and CP factors. High rainfall increases rain energy, making soil more susceptible to erosion, while steep slopes and land use with low vegetation coverage further exacerbate soil erosion. The integration of erosion rates parameters considers both long-term and short-term changes. Soil and slope characteristics undergo long-term changes, and thus, data for these parameters are used for erosion estimation across 2 periods. In contrast, rainfall and land use are highly dynamic parameters, requiring the use of different datasets. The erosion rate prediction is shown in Figure 13. The 2017 erosion estimation uses rainfall data from 2008-2016 and land-use classification from 2017, with an erosion rate ranging from 0 to 1984.9 tons/ha/year, with high erosion values observed on the volcanic slopes, while the volcanic fluvial plains are dominated by low erosion rates. The very heavy erosion hazard is less visible in the visualization but is identified at the peak of Lawu Volcano, whereas very light erosion is observed on the volcanic slopes and fluvial plains. The erosion estimations for 2024 range from 0 to 1174.61 tons/ha/year, as the R factor is based on rainfall data from 2015 to 2023. The high erosion rate at the peak of Lawu Volcano may be attributed to the debris flow phenomenon, a rapid mass movement triggered by heavy rainfall. It is known that the upper slopes and cone of Lawu Volcano contain loose soil materials, including silt and sand. The area of erosion

rate class shows distinct changes. In 2017, the distribution of erosion classes was as follows: very light erosion covered 16064 ha, light erosion 11845 ha, moderate erosion 5089 ha, heavy erosion 904 ha, and very heavy erosion 13 ha. In 2024, light and moderate erosion areas decreased to 10829 ha and 5057 ha, respectively. Meanwhile, very light erosion increased to 17056 ha, heavy erosion increased to 957 ha, and very heavy erosion increased to 16 ha. Erosion is a phenomenon that can lead to a decline in soil fertility, erosion of topsoil, and land degradation. The slight increase in very light erosion suggests that erosion control efforts from 2017 to 2024, combined with the expansion of built-up land and the preservation of standing vegetation, are contributing to the reduction of erosion. The results are presented in Figures 14 and 15. In Figure 14, very heavy erosion is not visible, but it is detected at the summit of Lawu Volcano. Heavy and moderate erosion appears to dominate the slopes of the volcano, while light erosion is evenly distributed from the upstream to the downstream areas of the Samin sub-watershed. Very light erosion is partially visible on the slopes of Lawu Volcano and dominates the downstream region of the Samin sub-watershed.

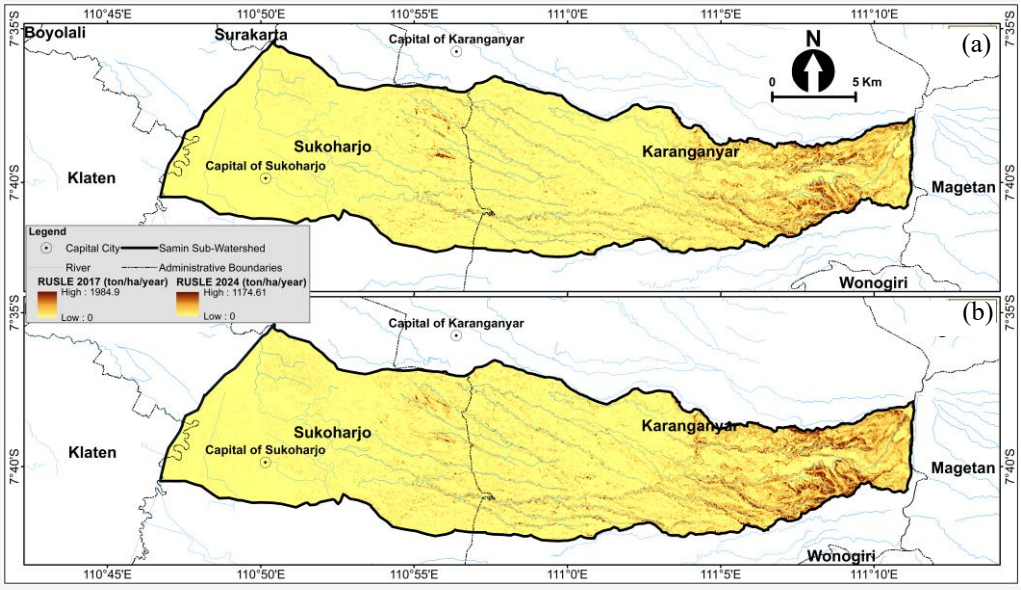

Figure 13: Soil Loss Erosion of Samin Sub-watershed (a) 2017, and (b) 2024

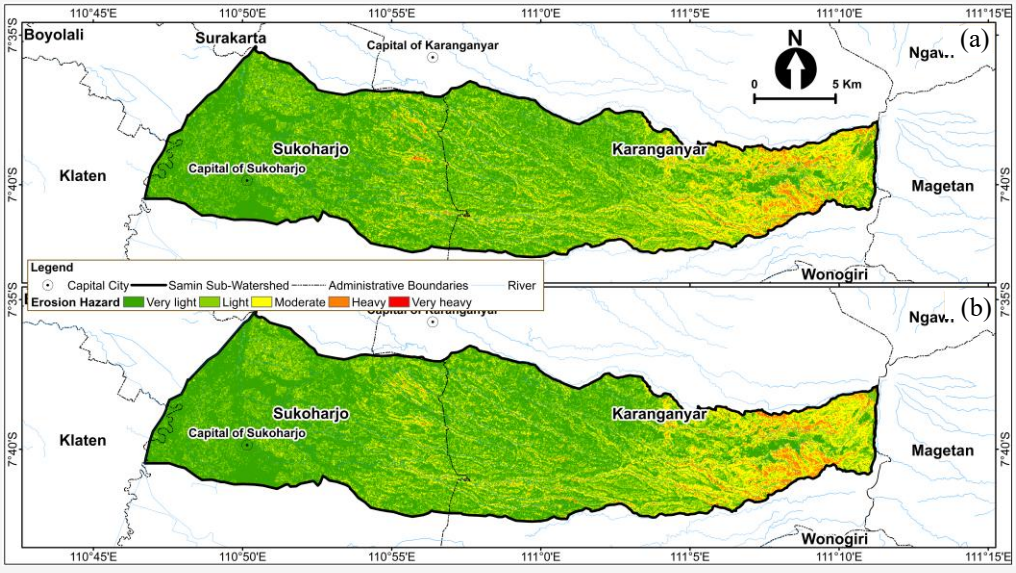

Figure 14: Erosion Hazards of Samin Sub-watershed (a) 2017, and (b) 2024

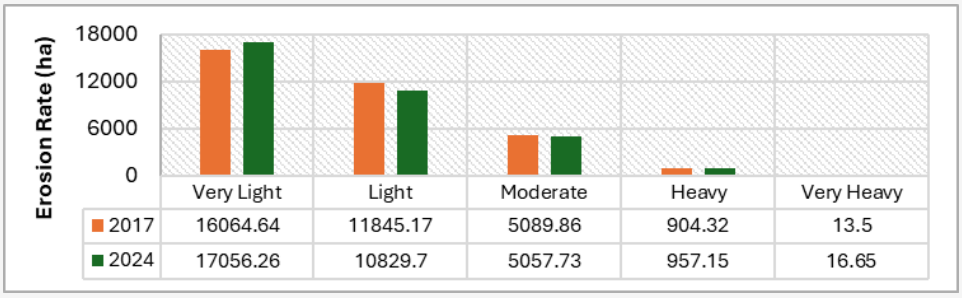

Figure 15: Erosion rate in Samin Sub-watershed

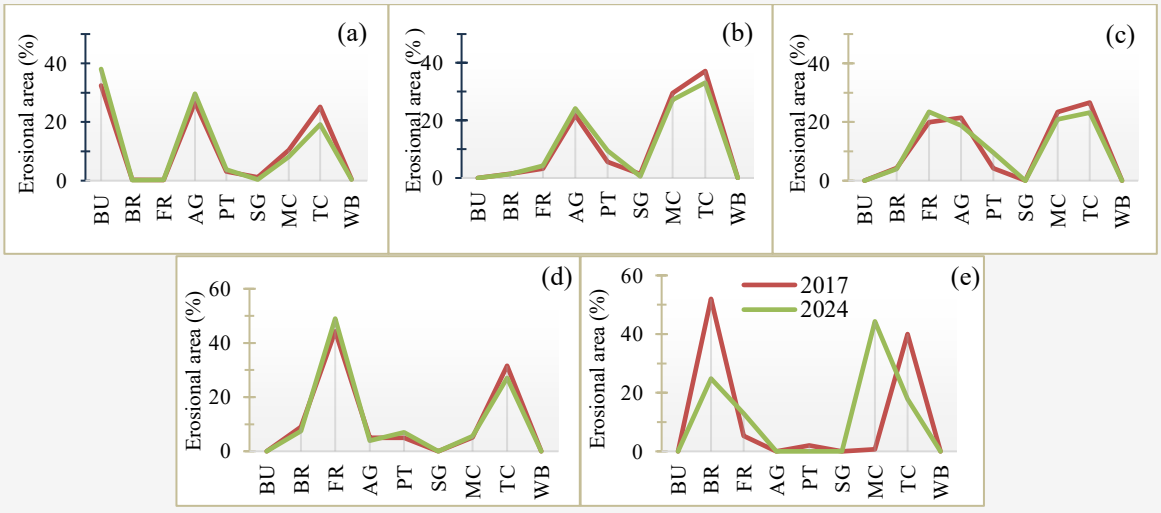

Figure 16: Comparison between erosion rate and land-use (a) very high (b) light (c) moderate (d) heavy, and (e) very heavy

4. Discussions

Empirical estimation of erosion rates using the RUSLE method, integrating the R, K, LS, and CP factors, has several limitations. Kriging spatial modeling for the R factor was based on only 11 data points, while the K factor relied on 20 soil samples selected according to landforms and slope variations. The spatial modeling results for the K factor shows a clear pattern in the central part of the Samin sub-watershed. However, kriging is highly sensitive to the number and distribution of samples, which limits its effectiveness and may lead to suboptimal spatial estimations. The impact of land-use changes on erosion hazards is illustrated in Figure 16. Very light erosion increases with agricultural land and terraced cropland. Similarly, built-up areas exhibit a high percentage of very light erosion, although this does not contribute to the reduction of erosion, as the land covered by buildings is not subject to surface runoff, thereby limiting the extent of eroded land. However, the expansion of built-up areas can have detrimental effects, such as reduced soil infiltration capacity and an increased potential for flooding. Light erosion is strongly influenced by changes in mixed cropland and terraced cropland, with minimal contributions from built-up areas and water bodies. Moderate erosion remains primarily influenced by cropland, with forests and agricultural land also playing a role, while built-up areas, shrub grasses contribute the least. Heavy erosion is largely influenced by forested land, while the contribution of agricultural land decreases. In contrast, bare land and terraced cropland show an increasing contribution to heavy erosion. Very heavy erosion is predominantly influenced by bare land, with cropland contributing to a lesser extent. Cropland demonstrates a significant influence on the erosion rates across various hazard classes, indicating that cropland practices with adequate land management contribute to the detachment and transportation of soil material through surface runoff. Mixed cropland, involving fields and a variety of crops, plays a dominant role in this process. Conservation efforts are crucial for reducing erosion rates, including the implementation of cover cropping and mulching. These practices help increase the organic matter content of the soil, thereby reducing soil erosion caused by rainfall and

surface runoff. Land-use changes and erosion, as key parameters of land criticality, are indicative of poor land condition. The impact of land-use changes on erosion rates is notably significant. Vegetated land plays a crucial role in reducing erosion rates, while bare land has a considerable impact on the risk of very heavy erosion. Areas of bare land and cropland with the potential for heavy erosion are located to the west of Lawu Volcano, which are associated with plantations, suggesting that these areas are in a replanting phase. During this phase, vegetation cover is significantly reduced, exacerbating erosion risks. The presence of bare land in 2017 notably reduced the land's ability to absorb water, leading to increased surface runoff. Additionally, the loss of topsoil contributed to a decline in soil fertility. Cropland with conservation terracing, which increased on the slopes of Lawu Volcano and downstream in 2017, helped mitigate the risk of very heavy erosion. Conversely, the rise in very heavy erosion in 2024 was influenced by the expansion of plantations and mixed cropland, both of which involve dry land farming practices. Standing vegetation cover plays a critical role in supporting the absorption and retention of surface water, as shown in 2024, where an increase in very light erosion is expected. Forests and agriculture, characterized by dense vegetation cover, can withstand high rainfall erosivity, thereby mitigating soil erosion. Moreover, dense vegetation cover is better at retaining and absorbing water, thereby reducing the transport of soil by surface runoff. Erosion estimation is conducted empirically using the RUSLE method, which indicates that steep slopes with loose soil material have a high potential for heavy erosion. Land-use with dense vegetation cover on steep slopes is particularly effective in reducing the impact of soil erosion, thereby helping to preserve soil fertility. Erosion rate estimation using an empirical approach and the RUSLE method demonstrates that land-use changes significantly influence the erosion rate. Land-use, as a CP factor, shows a Pearson correlation of 0.95 over the 2-year prediction period, which is higher than the modeling results based on the vegetation index as a C-factor, which has a correlation of 0.91 [23]. The combination of the vegetation index with DEM also provides a correlation of up to 0.95, but the modeling requires attention to soil spectral reflectance [24]. Land use, which defines bare land as a separate class, offers a different level of detail in the CP factor assessment.

The application of Random Forest classification to classify land-use and CP factors yielded good results, with the integration of spectral values and terrain characteristics achieving 92.01% overall accuracy in fieldwork. This provides a more representative basis for CP values across various terrain conditions and land-uses in the field. The ranking of variable importance in Random Forest classification indicates that both spectral values and terrain characteristics significantly contribute to improved modeling, despite the analysis being conducted at medium resolution and with limited data. Digital land-use classification is derived from the value of each pixel, whereas only the integration of various spectral bands can provide an overview of land-cover without considering terrain conditions. The contribution of various variables, however, allows for a more detailed classification.

Mapping land use changes is highly influential in estimating erosion rates, where increased land use with low CP factor values contributes to the reduction of erosion rates. Land-use mapping, when determining the CP factor for erosion rates, provides a more representative relationship between field observations and modeling. Mapping CP factors using Random Forest classification presents challenges, such as the need for detailed training samples, which affect the accuracy of land use classification. The accuracy of land-use classification, in turn, influences the accuracy of erosion rate estimation.

5. Conclusion

The empirical erosion rate, calculated using the RUSLE method, incorporates several factors: rainfall erosivity (R), soil erodibility (K), slope length and steepness (LS), and vegetation cover and conservation practices (CP). Among these, the R-factor and CP-factor are the most dynamic, as they fluctuate over time. Variations in these factors between different periods significantly affect the rate of soil loss. Land use classification, utilizing the Random Forest algorithm, integrates spectral data from Landsat-8 with elevation and slope data from the Alos Palsar DSM, achieving an overall accuracy of 92.01%. These classifications are then used to derive CP-factor values, which range from 0 to 1, with higher values indicating greater susceptibility to erosion. The estimated erosion rate in 2017 was 1984.9 tons/ha/year, while the projected erosion rate for 2024 is 1174.61 tons/ha/year. The differences in erosion rates are primarily attributed to variations in rainfall erosivity between the periods 2008-2016 and 2015-2023. A Pearson correlation analysis between erosion rates and CP factor values derived from land use classification revealed a coefficient of 0.95, indicating that 90% of the variation in erosion rates is significantly influenced by land use changes in the Samin sub-watershed. Land uses that contribute significantly to heavy erosion hazards include bare land and cropland (both mixed and terraced), with a

CP factor value of 0.25 or higher. In contrast, water bodies and built-up areas were assigned a CP factor value of 0, as they are not susceptible to erosion. Water bodies act as sedimentation zones, while built-up areas remain unaffected by erosion due to their coverage by impervious surfaces. These findings underscore the critical role of vegetation cover in reducing erosion rates, while land without vegetation cover is more vulnerable to higher erosion rates. However, this study has limitations in the spatial modeling of the R-factor and K-factor, both of which were interpolated using simple kriging with a limited number of data points. Nevertheless, the accuracy of land use classification directly affects the reliability of the erosion rate estimates.

Acknowledgement

The author sincerely thanks River Basin Management Office **(**BBWS) Bengawan Solo for providing the daily rainfall data and for granting permission to conduct fieldwork. Special thanks are due to the Faculty of Geography at Universitas Gadjah Mada under the PUAPT program for their invaluable support, guidance, and resources throughout this study. The author is also grateful to the editors for their careful consideration and constructive feedback, and to the anonymous reviewers for their insightful comments and suggestions, which significantly enhanced the quality of this work.

References

[1] Kironoto, B. A., Yulistiyanto, B. and Olii, M. R., (2020). *Erosi dan Konservasi Lahan*. Yogyakarta. [Erosion and Land Conservation. Yogyakarta]. Gadjah Mada University Press.

[2] Arsyad, S., (2012). *Konservasi Tanah dan Air*. [Soil and Water Conservation]. Bogor: IPB Press.

[3] Asdak, C., (2010). *Hidrologi dan Pengelolaan Daerah Aliran Sungai*. [Hydrology and Watershed Management.] Yogyakarta: Gadjah Mada University Press.

[4] Talib, N., Abdul Maulud, K., Mohd, F., Mohd Taib, A., and Abdullah, M. (2026). Assessing the Impact of Topography on Soil Erosion in Agricultural Areas Using UAV and GIS-Based Analysis. *International Journal of Geoinformatics*, Vol. 22(1), 47–55. https://doi.org/10.52939/ijg.v22i1.4719.

[5] Yanti, D. and Arlius, F., (2014). Analisis Spasial Konversi Lahan Pertanian Kota Padang tahun 2003-2012. [Spatial Analysis of Agricultural Land Conversion in Padang City 2003-2012]. *Jurnal Teknologi Pertanian Andalas*, Vol. 18, 25-33.

[6] Arifin, M., (2010). Kajian Sifat Fisik Tanah dan Berbagai Penggunaan Lahan dalam Hubungannya dengan Pendugaan Erosi Tanah. *Jurnal Pertanian MAPETA*, Vol. 12, 111-115.

[7] Zawiyah, Tjandra, M. A. and Yanti, D., (2025). Land-use Scenario Simulation for Erosion Control Using the Universal Soil Loss Equation (USLE) Method in Nagari Lawang, Agam Regency. *Jurnal Teknik Pertanian Lampung*, Vol. 14. https://doi.org/10.23960/jtep-l.v14i1. 262-272.

[8] Seeboonruang, U., Mandadi, R., Thammaboribal, P., Gonzales, A. L., Kanchan, A. and Ganni, S. V. S. A. B., (2025). Assessing the Combined Impacts of Future Climate and Land Use Changes on Soil Loss and Sediment Retention in the Lam Phra Phloeng Watershed, Thailand. *Agriculture*. Vol. 15. https://doi.org/ 10.3390/agriculture15232511.

[9] Fadhilla, S., Kusumandari, A. and Senawi, (2021). Soil Erosion Prediction using USLE Model in Cangkringan Micro Watershed Model, Yogyakarta. *IOP Conference Series: Earth and Environmental Science, Medan, Indonesia, August 24-25, 2021*, Vol. 912. https://doi.org/ 10.1088/1755-1315/912/1/012092.

[10] Seeboonruang, U., Mandadi, R., Thammaboribal, P., Gonzales, A. L., Kanchan, A., Ganni, S. V. S. A. B., (2026). Land Use Classification, Prediction, and the Relationship Between Land Use and Sediment Loss in the Lam Phra Phlong Watershed, Thailand. *Agriculture*. Vol. 16. https://doi.org/10.3390/ agriculture16040448.

[11] Nurlina, Kadir, S., Kurnain, A., Ilham, W. and Ridwan, I., (2022). Analysis of Soil Erosion and its Relationship with Land-use/Cover in Tabunio Watershed. *IOP Conf. Series: Earth and Environmental Science, Banjarbaru, Indonesia, October 23-24, 2024*, Vol. 976. https://doi.org/10.1088/1755-1315/976/1/0120 27.

[12] Rennard, K. G., Foster, G. R., Weesies, G. A., McCool, D. K. and Yoder, D. C., (1997). *Predicting Soil Erosion by Water: A Guide to Conservation Planning with the Revised Universal Soil Loss Equation (RUSLE)*. Agriculture Handbook No.573. [E-book] Available: https://www.tucson.ars.ag.gov/unit/publications/PDFfiles/717.pdf.

[13] Buraka, T., Elias, E., Suryabhagavan, K.V. and Lelago, A., (2024). Assessment of Soil Erosion Risks in Response to Land-use and Land-cover Changes in Coka Watershed, Southern Ethiopia. *Geology, Ecology, and Landscapes*, Vol. 8. https://doi.org/10.1080/24749508.2022.2109825.

[14] Seeboonruang, U., Mandadi, R., Thammaboribal, P., Gonzales, A. L., and Bharadwaz, G. S. V. S. A., (2025). Estimation of Soil Erosion and Enhancing Sediment Retention in the Lam Phra Phloeng Watershed: Insights from RUSLE and InVEST Modelling. *Water*, Vol. 17. https://doi.org/10.3390/w17233339.

[15] Belay, T. and Mengistu, D. A., (2021). Impacts of Land-use/Land Cover and Climate Changes on Soil Erosion in Muga Watershed, Upper Blue Nile Basin (Abay), Ethiopia. *Ecological Processes*, Vol. 10. https://doi.org/10.1186/s13717-021-00339-9.

[16] Lillesand, T. M., Kiefer, R. W. and Chipman, J. W., (2015). *Remote Sensing and Image Interpretation (7th ed)*. New Jersey: John Wiley and Sons.

[17] Lukyanchuk, K. A., Kovalchuk, I. P. and Pidkova, O. M., (2020). Application of a Remote Sensing in Monitoring of Erosion Processes. *Geoinformatics: Theoretical and Applied Aspects 2020*, Vol. 2020. https://doi.org/10.3997/2214-4609.2020geo131.

[18] Borrelli, P., Robinson, D. A., Fleischer, L. R., Lugato, E., Ballabio, C., Alewell, C., Meusburger, K., Modugno, S., Schutt, B., Ferro, V., Bagarello, V., Van Oost, K., Montanarella, L. and Panagos, P., (2017). An Assessment of the Global Impact of 21st Century Land-use Change on Soil Erosion. *Nature Communications*, Vol. 8. https://doi.org/10.1038/s41467-017-02142-7.

[19] Qiao, X., Li, Z., Lin, J., Wang, H., Zheng, S. and Yang, S., (2024). Assessing Current and Future Soil Erosion Under Charging Land-use based on InVEST and FLUS Models in the Yihe River Basin, North China. *International Soil and Water Conservation Research*, Vol. 12. https://doi.org/10.1016/j.iswcr.2023.07.001.

[20] Danoedoro, P., Widayani, P., Hidayati, I.N., Arjasakusuma, S., Gupita, D. D. and Salsabila, H. N., (2023). Vegetation Structural Composition Mapping of a Complex Landscape using Forest Cover Density Transformation and Random Decision Forest Classifier: A Comparison. *Geocarto International*, Vol. 38. https://doi.org/10.1080/10106049.2023.2220289.

[21] Danoedoro, P., Widayani, P., Hidayati, I. N., Kartika, C. S. D. and Alfani, F., (2024). Incorporating Landscape Ecological Approach in Machine Learning Classification for Agricultural Land-use Mapping Based on a Single Date Imagery. *Geocarto International,* Vol. 39. https://doi.org/10.1080/10106049.2024.2356844.

[22] Paul, S. S., Li, J., Li, Y. and Shen, L., (2021), Assessing Land Use–Land Cover Change and Soil Erosion Potential using a Combined Approach through Remote Sensing, RUSLE and Random Forest Algorithm. *Geocarto International*, Vol. 36. https://doi.org/10.1080/10106049.2019.1614099.

[23] Cheng, Z., Lu, D., Li, G., Huang, J., Sinha, N., Zhi, J. and Li, S., (2018). A Random Forest-based Approach to Map Soil Erosion Risk Distribution in Hickory Plantations in Western Zhejiang Province, China. *Remote Sensing*, Vol. 10. https://doi.org/10.3390/rs10121899.

[24] Sulistyo, B., Gunawan, T., Hartono and Danoedoro, P., (2009). Towards a Fully and Absolutely Raster-based Erosion Modeling by using RS and GIS. *Indonesian Journal of Geography*, Vol. 41, 149-170.

[25] Sulistyo, B., Gunawan, T., Hartono and Danoedoro, P., (2011). Pemetaan Faktor C yang diturunkan dari berbagai Indeks Vegetasi Data Penginderaan Jauh sebagai Masukan Pemodelan Erosi di DAS Merawu. [Mapping of C Factors derived from various Vegetation Indices of Remote Sensing Data as Input for Erosion Modeling in the Merawu Watershed]. *Jurnal Manusia dan Lingkungan*, Vol. 18, 68-78.

[26] Sulistyo, B., Gunawan, T., Hartono, Danoedoro, P. dan Listyaningrum, N., (2017). Absolute Accuracy of the Erosion Model of DEM-NDVI and it's Modification. *International Journal of Geoinformatics*, Vol. 13, 23-34. https://journals.sfu.ca/ijg/index.php/journal/article/view/1032.

[27] Arif, N., Danoedoro, P., Hartono and Mulabbi, A., (2020). Erosion Prediction Model using Fractional Vegetation Cover. *Indonesian Journal of Science and Technology*, Vol. 5. https://doi.org/10.17509/ijost.v5i1.21060.

[28] Arif, N., Danoedoro, P. and Hartono, (2017). Analysis of Artificial Neural Network in Erosion Modeling: A Case Study of Serang Watershed. *IOP Conference Series: Earth and Environmental Science, Yogyakarta, Indonesia, September 27-28, 2017*, Vol. 98. https://doi.org/10.1088/1755-1315/98/1/012027.

[29] Thammaboribal, P. (2024). Investigating Land Surface Temperature Variation and Land Use Land Cover Changes in Pathumthani, Thailand (1997-2023) using Landsat Satellite Imagery: A Comprehensive Analysis of LST and Urban Hot Spots (UHS). *International Journal of Geoinformatics*, Vol. 20(2), 27–41. https://doi.org/10.52939/ijg.v20i2.3063.

[30] USGS. *Landsat 5, USGS: Science for a Changing World*, Available: https://www.usgs.gov/landsat-missions/landsat-5. [Accessed Oct. 18, 2024].

[31] Thammaboribal, P., and Tripathi, N. (2024). Predicting Land Use and Land Cover Changes in Pathumthani, Thailand: A Comprehensive Analysis from 2013 to 2023 Using Landsat Satellite Imagery and CA-ANN Algorithm, with Projections for 2028 and 2038. *International Journal of Geoinformatics*, Vol. 20(5), 13–27. https://doi.org/10.52939/ijg.v20i5.3225.

[32] Roy, D. P., Kovalskyy, V., Zhang, H. K., Vermote, E. F., Yan, L., Kumar, S. S. and Egorov, A., (2016). Characterization of Landsat-7 to Landsat-8 Refelctive Wavelength and Normalized Difference Vegetation Index Continuity. *Remote Sensing of Environment*, Vol. 185. https://doi.org/10.1016/j.rse.2015.12.024.

[33] Chaves, M. E. D., Picoli, M. C. A. and Sanches, I. D., (2020). Recent Applications of Landsat 8/OLI and Sentinel-2/MSI for Land-use and Land Cover Mapping: A Systematic Review. *Remote Sensing*, Vol. 12. https://doi.org/10.3390/rs12183062.

[34] Niipele, J. and Chen, J., (2019). The Usefulness of Alos-Palsar DSM Data for Drainage Extraction in Semi-arid Environments in the Iishana Sub-basin. *Journal of Hydrology: Regional Studies*, Vol. 21. https://doi.org/10.1016/j.ejrh.2018.11.003.

[35] Nithesnirmal, S., Thilagaraj, P., Rahman, S. A. and Jegankumar, R., (2019). Erosion Risk Assessment through Morphometric Indices for Prioritisation of Arjuna Watershed using ALOS-PALSAR DSM. *Modeling Earth Systems and Environment*, Vol. 5, 907-924. https://doi.org/10.1007/s40808-019-00578-y.

[36] Khassaf, S. I. and Rammah, A. H., (2021). Estimation of Slope Length Faktor (L) and Slope Steepness Factor (S) of RUSLE Equation in the Euphrates River Watershed by GIS Modeling. *Kufa Journal of Engineering*, Vol. 9. https://doi.org/10.30572/2018/kje/090307.